AGU PUBLICATIONS

JGR

Journal of Geophysical Research: Atmospheres

RESEARCH ARTICLE
10.1002/2017JD027262

Assessment of NPP VIIRS Albedo Over Heterogeneous Crop Land in Northern China

Xiaodan Wu[1,2,3,4], Jianguang Wen[1], Qing Xiao[1], Yunyue Yu[5], Dongqin You[1], and Andreas Hueni[3]

[1]State Key Laboratory of Remote Sensing Science, Institute of Remote Sensing and Digital Earth, Chinese Academy of Sciences, Beijing, China, [2]College of Earth and Environmental Sciences, Lanzhou University, Lanzhou, China, [3]Remote Sensing Laboratories, University of Zurich, Zurich, Switzerland, [4]University of Chinese Academy of Sciences, Beijing, China, [5]NOAA/NESDIS/STAR, Camp Springs, MD, USA

Key Points:
- The accuracy of the latest albedo products, including VIIRS, GLASS, and MODIS (Collection 6) over heterogeneous surfaces, was evaluated and compared
- Ground-observed albedo from a wireless sensor network and an upscaling strategy specified for validation of VIIRS albedo were combined to derive ground references at pixel scale
- The VIIRS albedo has a high accuracy with a RMSE of 0.02 versus ground reference and successfully captures the rapid change of albedo by improving temporal resolution to daily

Correspondence to:
J. Wen,
wenjg@radi.ac.cn

Citation:
Wu, X., Wen, J., Xiao, Q., Yu, Y., You, D., & Hueni, A. (2017). Assessment of NPP VIIRS albedo over heterogeneous crop land in northern China. *Journal of Geophysical Research: Atmospheres*, *122*, 13,138–13,154. https://doi.org/10.1002/2017JD027262

Received 7 JUN 2017
Accepted 25 NOV 2017
Accepted article online 3 DEC 2017
Published online 20 DEC 2017

Abstract In this paper, the accuracy of Suomi National Polar-orbiting Partnership Visible Infrared Imaging Radiometer Suite (VIIRS) land surface albedo, which is derived from the direct estimation algorithm, was assessed using ground-based albedo observations from a wireless sensor network over a heterogeneous cropland in the Huailai station, northern China. Data from six nodes spanning 2013–2014 over vegetation, bare soil, and mixed terrain surfaces were utilized to provide ground reference at VIIRS pixel scale. The performance of VIIRS albedo was also compared with Global LAnd Surface Satellite (GLASS) and Moderate Resolution Imaging Spectroradiometer (MODIS) albedos (Collection 5 and 6). The results indicate that the current granular VIIRS albedo has a high accuracy with a root-mean-square error of 0.02 for typical land covers. They are significantly correlated with ground references indicated by a correlation coefficient (R) of 0.73. The VIIRS albedo shows distinct advantages to GLASS and MODIS albedos over bare soil and mixed-cover surfaces, while it is inferior to the other two products over vegetated surfaces. Furthermore, its time continuity and the ability to capture the abrupt change of surface albedo are better than that of GLASS and MODIS albedo.

1. Introduction

The surface albedo is defined as the ratio of the solar radiation reflected by the land surface to the radiation incident on the surface (Liang, 2004). It is a key parameter in climate and biogeochemical models as it determines the amount of solar radiation absorbed by the land surface. Remote sensing provides a unique method for obtaining albedos at regional and global scales. Efforts have been devoted to establish the methodologies to retrieve albedos from satellite remote sensing data, and significant progress has been achieved over the past few decades, including narrow-to-broadband conversions (Liang, Strahler, & Walthall, 1999), bidirectional reflectance distribution function (BRDF) angular modeling (Lucht et al., 2000; Schaaf et al., 2002; Wanner et al., 1997; You et al., 2015), direct-estimation algorithms based on linear regression models (Cui, Mitomi, & Takamura, 2009; He et al., 2012; Qu et al., 2014), and joint optimal algorithms to estimate albedos from geostationary satellite data (Govaerts et al., 2010). Albedo products have been generated using the above algorithms, including albedos derived from the advanced very high resolution radiometer (AVHRR) (Saunders, 1990), Moderate Resolution Imaging Spectroradiometer (MODIS) (Gao et al., 2005), Polarization and Directionality of Earth Reflectances (Bicheron & Leroy, 2000), Meteosat Second Generation (Govaerts et al., 2008; Leeuwen & Roujean, 2002), and Medium-Resolution Imaging Spectrometer (Muller, 2008).

The Suomi National Polar-orbiting Partnership (NPP) satellite was launched on 28 October 2011, and the Visible Infrared Imaging Radiometer Suite (VIIRS) on board the NPP satellite provides the majority of the environmental data records (Cao et al., 2013). The VIIRS albedo is derived from VIIRS top-of atmosphere (TOA) reflectance using an approach known as the direct estimation method (Wang et al., 2013), which estimates land surface albedos directly from TOA reflectance without using an atmospheric correction procedure (Liang, Stroeve, & Box, 2005). Unlike the previous direct estimation methods applied to the GLASS albedo products (Liang, 2003; Liang et al., 1999; Liang, Stroeve, & Box, 2005; Qu et al., 2014), VIIRS albedo algorithm has been significantly improved for a better retrieval quality. Multiple aerosol types and land surface bidirectional reflectance distribution functions (BRDFs) are incorporated in a radiative transfer simulation to develop the

regression models. Therefore, the developed surface-specific look-up tables (LUTs) depend on the surface BRDFs (Wang et al., 2013), and they improve the accuracy of the albedo estimates.

Albedo products from different sensors have been used successfully in many scientific fields, for example, to simulate rainfall processes (Shi et al., 2009), air temperature (Li, Sheng, & Zhao, 2012), and climate simulations (Strugnell, Lucht, & Schaaf, 2001). In particular, albedo products generated by AVHRR, MODIS, and VIIRS can aid the development of climate data record albedo time series (Privette et al., 2004; Yu, Privette, & Pinheiro, 2008). However, albedo products are not widely used via direct analyses or data assimilation in climate and environmental research because of the lack of detailed information on the accuracy. Thus, validations of different albedo products are necessary to provide albedo users with data accuracy information, to identify possible deficiencies and to propagate such uncertainties into climate models. Many studies have been conducted to evaluate the accuracies of the MODIS and AVHRR albedo products (Muller et al., 2007; Chen et al., 2008; Liu et al., 2009; Román et al., 2009; Wang & Zender, 2010; Cescatti et al., 2012; Wang et al., 2012; Roman et al., 2013; Q. Liu, Wang, et al., 2013; He et al., 2014); however, the evaluation of VIIRS albedo has just begun (Wang et al., 2013; Zhou et al., 2016).

Preliminary validations of VIIRS albedo have demonstrated that VIIRS albedo has a root-mean-square-error (RMSE) of 0.020 and a slight negative bias of 0.004 compared with the ground measurements (Wang et al., 2013). However, these assessments have been carried out by direct comparison with single site measurements under the general assumption that the ground albedo has such a good spatial representativeness that it can be directly used to validate the VIIRS albedo product. The primary challenge, however, is that most sites with heterogeneous surfaces are invalid for direct comparison with VIIRS albedo because of their limited spatial representativeness. The term of spatial representativeness here denotes the degree to which a ground-observed albedo is able to represent the surrounding landscape extending to the satellite footprint. To assess the accuracy of VIIRS albedo over heterogeneous surfaces, Zhou et al. (2016) have introduced the intermediate scale albedo data, that is, Landsat albedo, as bridges to fill gaps between ground measurements and VIIRS albedo products. However, this kind of validation strategy is faced with many types of uncertainties, which are the result of additional inversion or geometric registration errors (Peng et al., 2014). Therefore, the absolute accuracy of VIIRS albedo products can suffer from the effects of error propagation (Wu et al., 2016).

The main obstacles confronting the validation of VIIRS granule-based albedo over heterogeneous land surfaces arise from two aspects: (a) the in situ albedo may not represent the mean albedo at the VIIRS pixel scale as it is usually acquired at a small local scale, and (b) even for a spatially representative site, the fixed position of the in situ sensor makes it difficult to represent the landscape at the VIIRS pixel scale as the spatial extent of the VIIRS pixel corresponding to the site varies with repeated acquisitions.

Currently, a wireless sensor network (WSN), established by the State Key Laboratory of Remote Sensing Science of China, offers the possibility of assessing the accuracy of VIIRS swath-based albedo at flexible temporal and spatial scales (Dou et al., 2016). The optimization of the WSN node locations, the upscaling method of ground measurements, and the validation strategy for gridded albedo products have been developed (Wu et al., 2016). This paper focuses on the evaluation of the VIIRS swath-based albedo using ground observed albedo by improving the existing upscaling method. As the continuation of the surface products provided by MODIS instruments, the performance of VIIRS albedo was also compared with that of GLASS and MODIS albedo, as they were both derived from MODIS reflectance and with similar spatial resolutions.

A brief description of the VIIRS albedo provisional product and its retrieval algorithms was given in section 2. The ground albedo measurements collected in the Huailai WSN experiment, the ground data processing method, and the satellite data were described in section 3. The results of the VIIRS albedo evaluation and comparison with GLASS and MODIS albedo (V005 and V006) are presented in section 4. Finally, the conclusions of this paper are summarized in section 5.

2. VIIRS Albedo

2.1. VIIRS Albedo Algorithm

The direct estimation algorithm is currently employed as the unique algorithm to generate VIIRS albedo products (Wang et al., 2013). It is a regression approach used for both the bright surfaces, such as

Table 1
Basic Specifications of the Bands to Estimate Surface Albedo (Liang, Yu, & Defelice, 2005)

Band name	Spectral range (nm)	Center (nm)	Width (nm)
M1	402–422	412	20
M2	436–454	445	18
M3	478–498	488	20
M4	545–565	555	20
M5	662–682	672	20
M7	846–885	865	39
M8	1,230–1,250	1,240	20
M10	1,580–1,640	1,610	60
M11	2,225–2,275	2,250	50

snow, desert, and bare soils, and dark surfaces, such as vegetation. Nine bands (Table 1) from VIIRS were initially used to estimate land surface albedo. Because of the strong correlation among the bidirectional reflectance factors in bands 1–3, the M2 and M3 bands were excluded.

The algorithm estimates the surface albedo directly from VIIRS TOA reflectance in seven spectral bands using a linear regression function *f*:

$$A(\theta) = f(\rho_1(\theta, \vartheta, \phi), \rho_2(\theta, \vartheta, \phi), \ldots, \rho_n(\theta, \vartheta, \phi)) \quad (1)$$

where A is the broadband albedo, ρ is the TOA reflectance, and n indicates the seven VIIRS bands, M1, M4–5, M7–8, and M10–11. θ, ϑ, and ϕ are solar zenith angle, view zenith angle, and relative azimuth angle, respectively.

The coefficients of *f* are derived by a linear regression between land surface albedos and TOA reflectances, where the latter were generated from a VIIRS BRDF database (Qu et al., 2014; Wang et al., 2013) using the 6S (second simulation of a satellite signal in the solar spectrum) radiative transfer simulation (Kotchenova et al., 2006) for each combination of surface, atmosphere (aerosol types and aerosol optical depth (AOD)), and illumination and viewing geometry (represented by the solar zenith angle (SZA), the view zenith angle (VZA), and relative azimuth angle (RAA)).

During the TOA reflectance simulation process, five types of aerosol, including urban, rural, desert, biomass burning, and mixed all-type aerosol, were considered. Compared with the previous direct estimation methods (Liang et al., 1999; Liang, Stroeve, & Box, 2005; Qu et al., 2014), the major improvement of VIIRS albedo algorithm was considering the unique BRDF of bare soil and snow surfaces. The bare soil-specific LUT and snow-specific LUT were established by mainly using the BRDF of bare soil and snow in the simulation process, respectively (Wang et al., 2013; Zhou et al., 2016). Preliminary validation results over desert and snow surfaces have shown that the surface-specific BRDF LUT performs much better than that obtained from generic LUT, which is derived using all data in the BRDF database during the simulation process (Zhou et al., 2016).

2.2. VIIRS Albedo Product

VIIRS albedo product provides broadband blue-sky surface albedo at the VIIRS moderate resolution (approximately 750 m at nadir) every day. It is a granular product similar to the MODIS level 2 swath products. The pixels were flagged as either "confidently clear," "probably clear," "probably cloudy," or "confidently cloudy" using the VIIRS Cloud Detection. In this paper, only the albedos identified as "confidently clear" were used. Given the effect of adjacent clouds, two clear-sky conditions were considered. The "strict clear-sky" constraint used for the VIIRS albedo generation requires that both the pixel to be validated and its eight adjacent pixels are "confidently clear." The "clear-sky" condition requires the pixel to be validated to have a "confidently clear" status regardless of whether its neighbor pixels are clear or not.

Based on our requirements, the Liang research team at the Department of Geographical Sciences, University of Maryland, produced VIIRS albedo data for the Huailai test station in China. The data set includes albedo, cloud mask information, SZA, VZA, and RAA. The data span from day of year (DOY) 182, 2013 to DOY 212, 2014. There were usually two or more observations of the experimental area each day due to swath overlaps (Cayula, Arnone, & Vandermeulen, 2015). However, observations with SZAs larger than 70° were discarded because the VIIRS albedo is not reliable at higher SZAs (Wang et al., 2013). VIIRS moderate-band geolocation Sensor Data Records with a 750 m spatial resolution were used to identify the footprint of each VIIRS observation corresponding to the study area. Additionally, the satellite overpass time, SZA, and Land Quality Flag of the VIIRS albedo were also extracted.

3. Experimental Data

3.1. The In Situ Albedo

3.1.1. Ground Site and WSN Observation

The experiment was performed at the Huailai test station, Hebei province, China. A 2 km × 2 km area around the station (115.78°E–115.80°E and 40.35°N–40.37°N) was selected as the albedo product validation region (Figure 1). This area is characterized by its distinct land uses: bare soil between January and April, corn

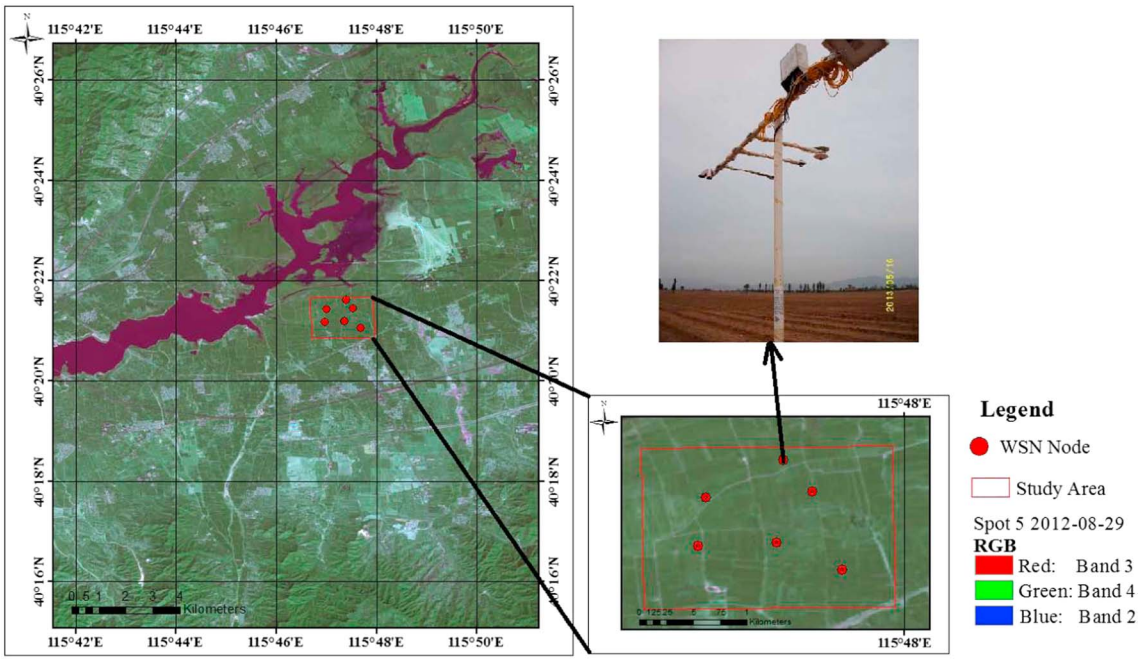

Figure 1. Top-of-atmosphere shortwave reflectance false color composite (SPOT, bands 3-4-2) surrounding the study area on 29 August 2012. The red rectangle shows the spatial extent of the study area, which covers a 2 km × 2 km area. The red points indicate the spatial distribution of WSN nodes.

from May to October, and occasional straw burning during November and December. During the growing season, corn growth is inconsistent because of differences in management (e.g., seeding time, irrigation, and fertilization). During the dormant season, the degree of heterogeneity increases because the surface is either a mixture of withered corn stalk and bare soil or a mixture of darker ash and bare soil caused by burning straw.

The locations of WSN nodes (Figure 1) were optimized based on the indicator of spatiotemporal representativeness (Wu et al., 2016) to capture the spatial-temporal variations of surface albedo over the region. Each WSN node was instrumented with two CNR pyranometers mounted back-to-back (Figure 2), which measured the total downward and upward radiation. The pyranometers were equipped with filter domes that provided a nearly perfect linear spectral response within the broadband range (0.3–2.8 μm). They were mounted at a height of 3 m. The footprints of the pyranometers depended on their heights above the underlying surface and were estimated to be ranging from 26.1 m to 8.7 m in diameter (Sailor, Resh, & Segura, 2006) with the growth of crop. The pyranometers took radiation measurements every 5 min, and the ground-based albedo observations could be precisely synchronized with the satellite overpass.

Figure 2. Photographs of WSN sites (node 5 for example) in different periods. (left to right) These pictures indicate the surface conditions during vegetation period, mixed surface period, and bare soil period, respectively.

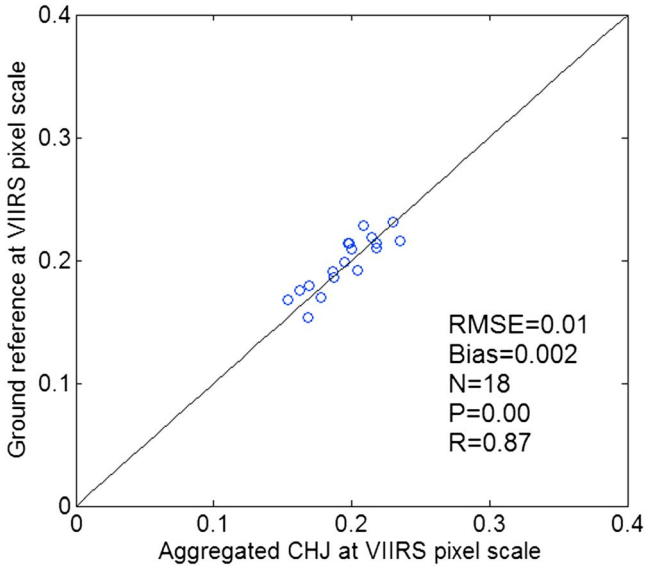

Figure 3. Scatterplot of ground reference at VIIRS pixel scale and aggregated CHJ albedo in the VIIRS pixel during the experimental period.

3.1.2. VIIRS-Pixel Ground Albedo Estimation and Evaluation

The WSN node observed albedo was calculated using the ratios of the 25 min averaged downward and upward radiations around the time of the NPP satellite overpass. Using this averaged irradiance (rather than instantaneous value) to construct the ground surface albedo can reduce random errors caused by wind and other disturbance (Wang & Zender, 2010).

The ground node observation was upscaled to VIIRS pixel scale by assigning different weight coefficients to different nodes, where the weight coefficients were generated statistically with the historical Huan Jing (HJ) albedo (equation (2)). The HJ albedos from 2010 to 2012 were generated from HJ images using the angular bin (AB) algorithm (Qu et al., 2014), provided along with the black-sky (BSA) and white-sky albedo (WSA) at a spatial resolution of 30 m. HJ blue-sky albedo (short for HJ albedo) was calculated by weighting the WSA and BSA with the ratio of diffuse radiation, which is dependent on the solar zenith angle (SZA) and the atmospheric optical depth (AOD). The AOD information was obtained from MODIS 10 km aerosol products (Collection V005, at 550 nm).

$$A_{pixel} = \sum_{i=1}^{n} \alpha_i w_i \quad (n = 1,\ 2,\ 3,\ 4,\ 5,\ 6) \tag{2}$$

where A_{pixel} refers to the aggregated calibrated HJ albedo (CHJ) corresponding to the spatial extent of VIIRS pixel to be validated, α_i is the HJ pixel albedo at the WSN node, n denotes the number of WSN nodes, and w_i is the upscaling weight coefficients to be derived with the ordinary least squares method. Considering the probability that a WSN node cannot provide an effective observation due to instrument failure or its limited spatial representativeness, the weight coefficients are calculated for all possible combinations of the WSN nodes and stored in a look-up table (LUT) (Wu et al., 2016). For example, the data from node 3 were excluded because of their poor quality. It should be noted that, as the footprint of the VIIRS albedo pixel over the study area was changing with different overpass time due to its swath-based storage format, the underlying surface for the pixel to be validated changed accordingly. Considering the surface heterogeneity, the surface albedo A_{pixel} corresponding to the VIIRS pixel was different for each satellite overpass, even for two adjacent observations. As a result, the upscaling weight coefficient LUT derived from equation (2) varied with each VIIRS

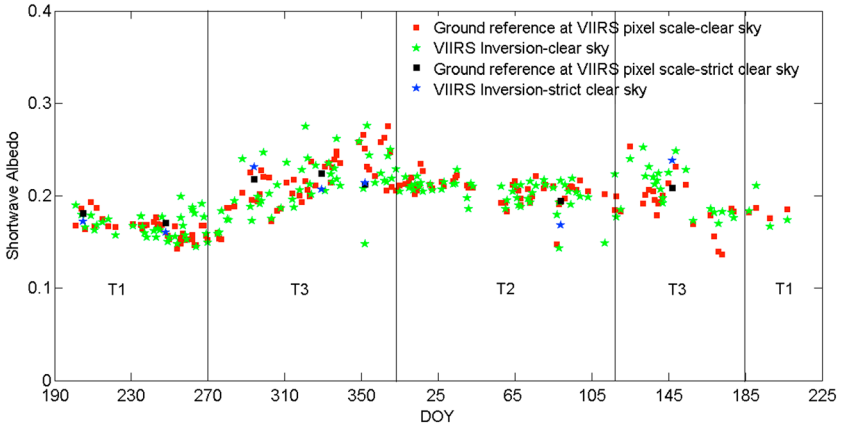

Figure 4. Time series of the instantaneous ground reference and VIIRS daily instantaneous albedo data. The red and black squares denote the ground reference in clear-sky and strict clear-sky conditions, respectively. The green and blue stars represent the VIIRS daily albedo in clear-sky and strict clear-sky conditions, respectively. The VIIRS albedos are more fluctuant than ground reference in time series.

Figure 5. Photographs of the land surface cover during (a) vegetation period, (b) mixed surface period resulted from a mixture of withered crops and bare soil, (c) mixed surface period due to a mixture of bare soil and darker ashes caused by straw burning, (d) bare soil period, and (d) mixed surface period with a mixture of vegetation and bare soil.

observation. After this step, the ground reference value at the VIIRS pixel scale can be derived by assigning the upscaling weight coefficients to WSN nodes' observations combined with a quality control process (Wu et al., 2016).

The accuracy of the ground reference value at VIIRS pixel scale was assessed by comparing the aggregated CHJ within the footprint of VIIRS pixel to the ground reference (Figure 3) during the experimental period (2013–2014). The ground reference and the aggregated CHJ at VIIRS pixel scale are significantly correlated with a correlation coefficient (R) of 0.87 and P value (F test) of 0. The RMSE and average bias are 0.01 and 0.002, respectively, which demonstrate the high accuracy of ground reference at VIIRS pixel scale.

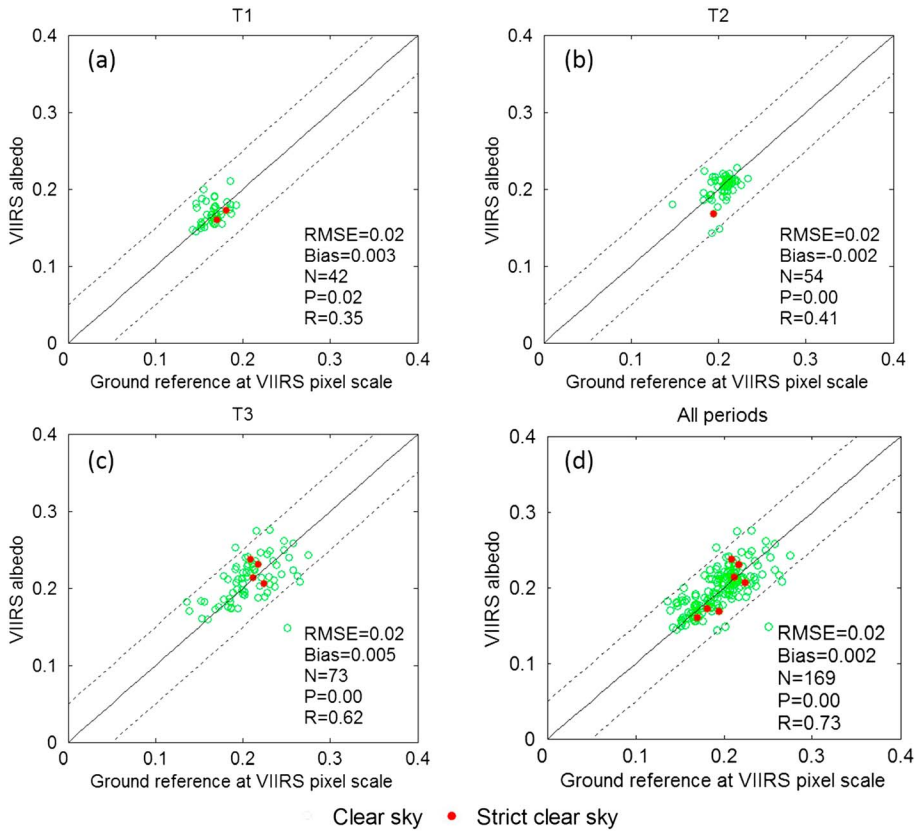

Figure 6. Scatterplots between the instantaneous ground reference and VIIRS instantaneous albedo under strict clear-sky and clear-sky conditions. The red solid circles and the green open circles indicate the strict clear-sky and clear-sky conditions, respectively. The dotted lines show the bias on the interval [−0.05, 0.05].

Table 2
Summary of the Evaluation Results for the VIIRS Instantaneous Albedo

	T1 (vegetation period)	T2 (bare soil period)	T3 (mixed cover period)	All periods
RMSE	0.02	0.02	0.02	0.02
Bias	0.003	−0.002	0.005	0.002
R	0.35	0.41	0.62	0.73
P	0.02	0.00	0.00	0.00
N	42	54	73	169

3.2. The GLASS and MODIS Albedo Product (Collection 5 and 6)

The 1 km GLASS albedo was derived from MODIS/Terra and Aqua satellite data with the angular bin (AB) algorithm (Qu et al., 2014). The intermediate products are retrieved daily and averaged using STF (Statistics-based Temporal Filtering) (N. F. Liu, Liu, et al., 2013) to generate an 8 day final product. For the consistency with the temporal resolution of VIIRS albedo, this paper just utilized the GLASS daily preliminary product.

The MODIS albedo product was estimated using the kernel-driven RossThick-LiSparse-Reciprocal model (Li & Strahler, 1992; Ross, 1981; Schaaf, Wang, & Strahler, 2011) to characterize anisotropic reflectivity of land surfaces (Lucht, Schaaf, & Strahler, 2002; Wanner et al., 1997). Instead of the 8 day temporal resolution of V005, the V006 collection is a daily albedo, with observations of the single day of interest emphasized (Mira et al., 2015; Wang et al., 2014). Unlike the NPP VIIRS swath-based instantaneous blue-sky albedo at the overpass time, both the GLASS and MODIS albedo provide the gridded BSA corresponding to the solar angle at local noon and WSA, and their blue-sky albedos were calculated by weighting the BSA and WSA with the proportions of the diffuse sky radiation arriving at the ground.

4. Results and Discussion

4.1. Consistency Assessment With In Situ Albedo

4.1.1. Daily Instantaneous Albedo

Figure 4 shows the annual time series of the VIIRS daily instantaneous albedo and the ground reference at the VIIRS pixel scale in the validation region. According to the land use, the experimental period was artificially divided into three time periods: vegetation period (T1, from 18 July to 30 September 2013 and from 1 to 31 July 2014), bare soil period (T2, from 1 January to 30 April 2014), and mixed surface period (T3, from 1 October to 31 December 2013 and from 1 May to 30 June 2014). The mixed surface period contains two cases (Figure 5): the corn harvest period, during which part of the area was covered by withered corn stalks or burned straw, and the seeding time, during which the corn had just begun to grow and frequent farm management (irrigation, fertilization, etc.) occurred, and inconsistencies in the growth increased the surface heterogeneity.

Both the ground reference and VIIRS albedo varied seasonally with vegetation phenology and changes in land cover. The VIIRS albedo agrees in general quite well with the ground reference throughout the year. However, an abnormal low value of VIIRS albedo is observed around DOY 350, where it was about 0.1 lower

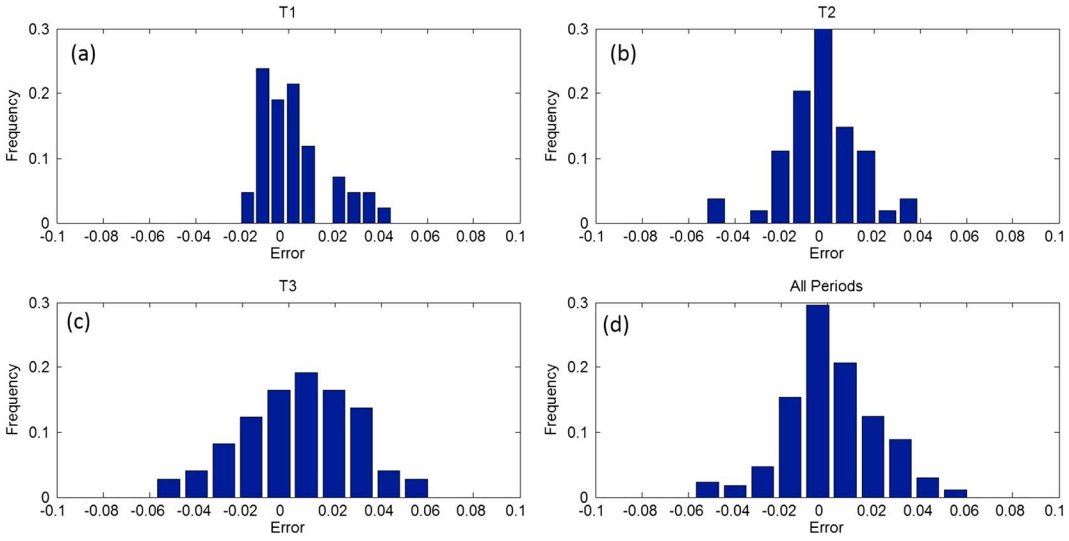

Figure 7. The distribution of the VIIRS instantaneous albedo errors (VIIRS albedo minus ground reference) during the different periods.

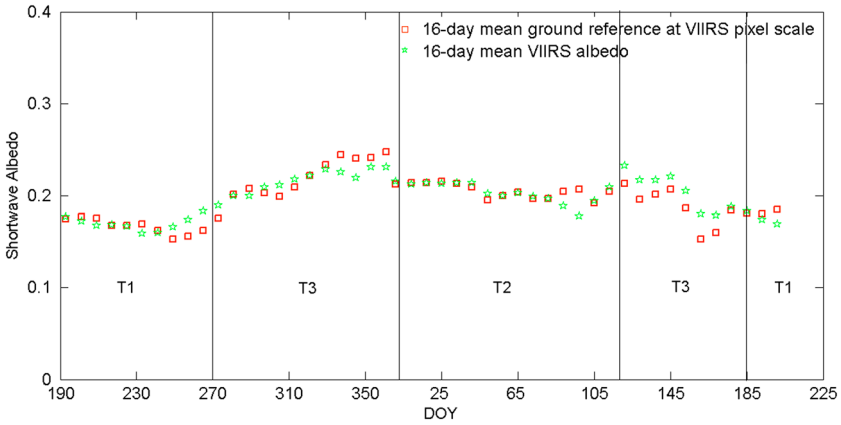

Figure 8. Time series of the 16 day mean *g*round reference (represented by red open squares) and 16 day mean VIIRS daily instantaneous albedo (denoted as green open stars), showing a better agreement throughout the year.

than the ground reference. It is caused by cloud shadow and excluded from the following analysis for a fair comparison.

Figure 6 shows scatterplots of the VIIRS albedo and ground reference during the different periods. The quantitative comparisons of the VIIRS albedo and the ground reference at the VIIRS pixel scale are summarized in Table 2. The mean difference (bias) and RMSE are used to measure the difference of the two kinds of albedo. The correlation coefficient (*R*) and significance value (*P*) are used to measure their consistency. *N* indicates the amount of data in the plot. It is noted that there are not enough strict clear-sky cases for the VIIRS albedo, and the statistical results under strict clear-sky condition are not statistically significant and are thus omitted.

RMSEs during the three periods (T1, T2, and T3) are all as low as 0.02, which demonstrates a high accuracy of VIIRS albedo over different kinds of land cover. The *P* values decrease from 0.02 (in T1) to 0.00 (in T2 and T3), which shows that the relationships between ground reference and VIIRS albedo during bare soil and mixed cover periods are more significant than that during the vegetation-covered period. Despite the low *R* of 0.35 during vegetation-covered period, the VIIRS albedo is consistent with ground reference since most of the data points are on the line 1:1. The average biases are slightly different during the three periods, which varies from 0.003 (T1) to −0.002 (T2) and then to 0.005 (T3). Most errors are distributed around 0, and the largest value is no more than 0.06 (Figures 7a–7c).

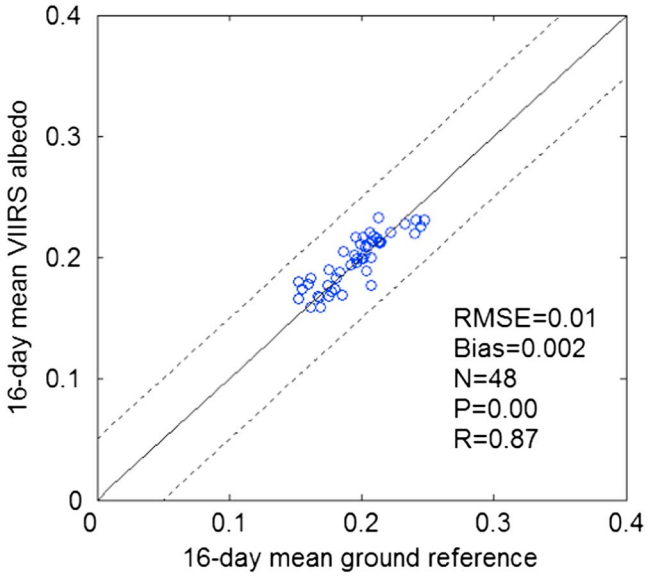

Figure 9. Scatterplot between the 16 day mean ground reference at the VIIRS pixel scale and 16 day mean VIIRS albedo. The dotted lines show the bias on the interval [−0.05, 0.05].

A combined analysis of all periods shows that the VIIRS albedo neither systematically overestimates nor underestimates the ground reference on the annual basis (Figure 6d). The errors are generally following approximately a normal distribution with a mean value of 0.002 (Figure 7d). The overall RMSE is 0.02, which indicates the high overall accuracy of VIIRS albedo. The *P* value of 0.00 and *R* value of 0.73 manifest the significant consistency between VIIRS albedo and ground reference.

The results in Figure 4 show that during the vegetation and bare soil periods, both the VIIRS albedo and ground reference temporal sequence are relatively smooth, even though the footprint of the swath data varies between acquisitions. This is because the land cover is relatively stable and homogeneous, and the signals are not significantly changed with variations of the footprint. The two kinds of albedos are very close in magnitude, indicated by most of the data points being distributed around the line 1:1 (Figures 6a and 6b). However, during the mixed terrain surface-covered period, they both noticeably fluctuate. This can be attributed to two aspects: one is the frequent change of the land cover; the other is the variation of the signals from different footprints, because the surface is significantly heterogeneous during this period and even a

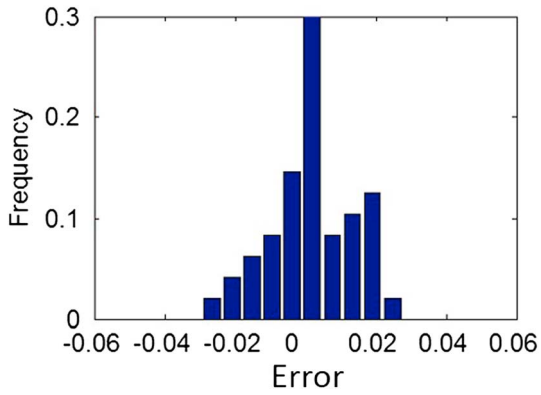

Figure 10. The distribution of the 16 day mean VIIRS albedo errors (16 day mean VIIRS albedo minus 16 day mean ground reference).

tiny change of footprint can result in large differences in albedo values. It is noteworthy that the volatility in the VIIRS albedo is greater than that of the ground reference. The scatterplots during T3 are dispersed, and the closeness between the VIIRS albedo and ground reference is not as good as for T1 and T2, despite T3 having a large *R* of 0.62, which is the result of the large variance of the distribution of surface albedo as shown in Figure 6c. As has been demonstrated previously in Zhou et al. (2016) and Qu et al. (2014), the disagreements are mainly caused by atmospheric effects, the limitations of the retrieval algorithm, and the failure of the cloud/shadow detection of VIIRS albedo. The results of the comparison indicate that the VIIRS albedo provides high-quality results during the vegetation-covered and bare soil-covered periods when the land surface is relatively stable. However, its stability decreases during the mixed-cover period when the surface changes frequently, although the VIIRS albedo is able to reveal rapid changes to some extent with an acceptable accuracy.

4.1.2. Sixteen-Day Mean Albedo

The 16 day VIIRS albedos were averaged to obtain the 16 day mean VIIRS albedo with an interval of 8 days, corresponding to the temporal step of the MODIS albedo (V005). The 16 day VIIRS albedo is closer to the 16 day ground reference than the VIIRS daily instantaneous albedo throughout the year (Figure 8). These two kinds of albedos are still significantly correlated as the *P* value is still equal to 0.00. Also, the RMSE decreases from 0.02 to 0.01, while *R* increases from 0.73 to 0.87 (Figure 9). The errors are concentrated in 0, and more than 90% of them are within the range of ±0.02. Only approximately 5% of the errors are distributed around −0.03 (Figure 10). These results indicate that some random errors in the ground reference and satellite albedo product can be reduced in the temporal aggregation, which led to a better agreement between them.

4.2. Consistency Assessment With the GLASS and MODIS Albedo (V005 and V006)

4.2.1. Comparison With GLASS and MODIS Daily Local Noon Albedo (V006)

The clear-sky GLASS local noon albedo was extracted and compared with the ground reference at a 1 km pixel scale (Figure 11), which was calculated from the WSN albedo at local solar noon with the upscaling coefficients by Wu et al. (2016). Abrupt changes in surface albedo can be observed from the ground reference but not from GLASS albedo. Additionally, GLASS albedo suffered from some missing data. The missing GLASS albedo data during DOY 27–70 were caused by the quality flag check process, which screened poor quality data. Their agreement is significantly good during T1, with a low RMSE of 0.01 and high *R* of 0.71 (Figure 12a). However, the agreement deteriorates in T3 as the RMSE increases to 0.03. The consistency is

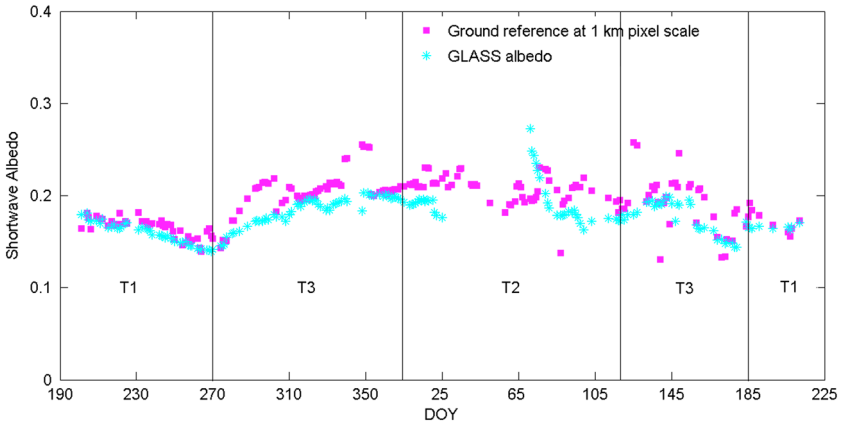

Figure 11. Time series of the local noon ground reference at 1 km scale (denoted as purple squares) and the GLASS daily local noon albedo (indicated by cyan asterisks). Data missing can be observed in GLASS albedo, but not in the ground reference.

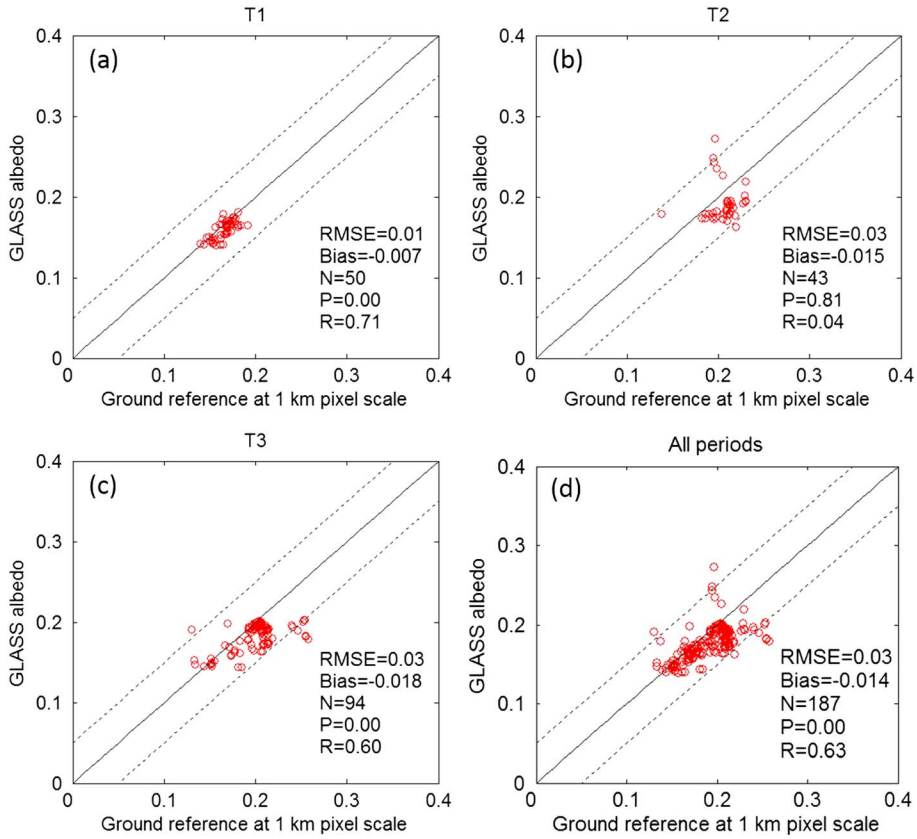

Figure 12. Scatterplots between the 1 km pixel scale ground reference and GLASS daily local noon albedo under clear-sky condition during the different periods. The dotted lines show the bias on the interval [−0.05, 0.05].

the worst in T2 (Figure 12b) with almost no correlation between in situ and GLASS albedos. The combined periods (Figure 12d) show an acceptable accuracy of GLASS albedo. The low *P* of 0.00 and *R* of 0.63 indicate a significant overall correlation between the GLASS albedo and the ground reference.

A comparison of *R* during T1 shows that the VIIRS instantaneous albedo estimates ($R = 0.35$) are poorer than the GLASS daily local noon albedo estimates ($R = 0.71$). The scatterplots of the VIIRS albedo are more dispersed than those of GLASS albedo, which may be the result of a laxer quality control (e.g., cloud/shadow detection) of the VIIRS albedo. During T2, the VIIRS albedo is closer to the ground reference than the GLASS albedo as indicated by the lower RMSE of 0.02 and higher R of 0.41 (GLASS albedo: RMSE = 0.03, $R = 0.04$). The temporal trend of the ground reference and VIIRS albedo is more consistent than the one of GLASS albedo. These results occur because the VIIRS albedo algorithm used a specific bare-soil BRDF LUT.

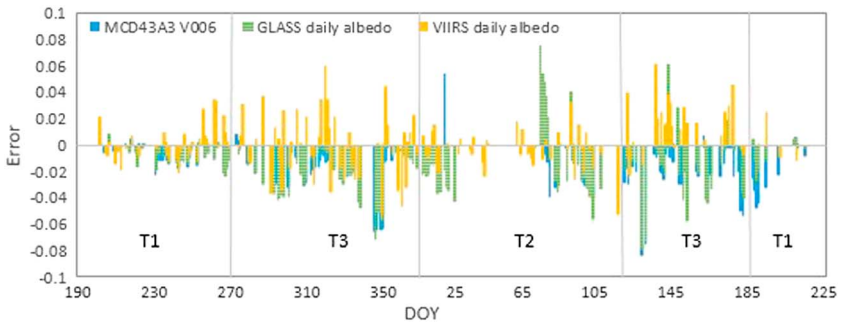

Figure 13. The comparison of the errors of MCD43A3 (V006), GLASS daily local noon albedo, and VIIRS daily instantaneous albedo with respect to the ground reference at corresponding time and pixel scale.

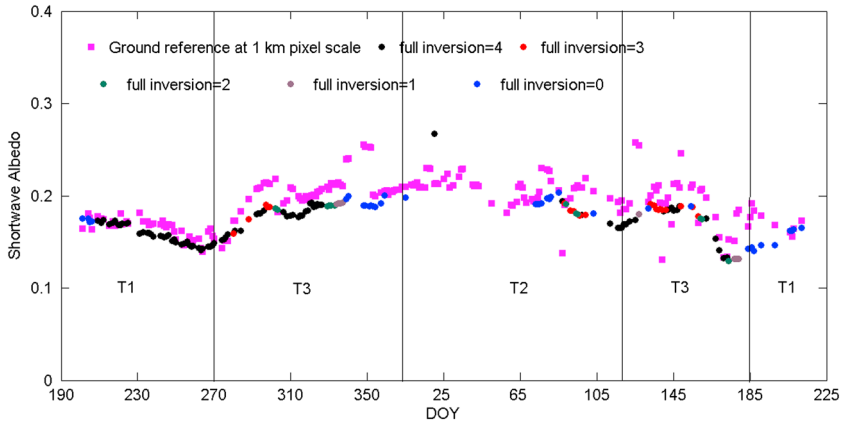

Figure 14. Comparisons between local noon ground reference at a 1 km scale and 1 km MODIS albedo (V006). The circles are color coded by the different number of MCD43A3 (V006) pixels used in full inversion within the 1 km scale.

During the mixed cover period, the RMSE (0.02) and average bias (0.005) of the VIIRS albedo are better than those of GLASS albedo (0.03 and −0.018), although the VIIRS and GLASS albedos have similar *R* values. High values in surface albedo are captured by VIIRS instantaneous albedo, but not by GLASS local noon albedo. On the whole, VIIRS albedo shows a higher overall accuracy with a smaller RMSE and a larger *R* than GLASS albedo.

Comparison of the time series of VIIRS and GLASS albedo shows a number of differences. First, the fluctuation range of VIIRS albedo in time series is larger than that of ground reference (VIIRS pixel scale); on the contrary, the GLASS albedo temporal sequence is smoother than that of ground reference (1 km pixel scale). This is because the GLASS albedo was smoothed using the STF method (N. F. Liu, Liu, et al., 2013), but the VIIRS

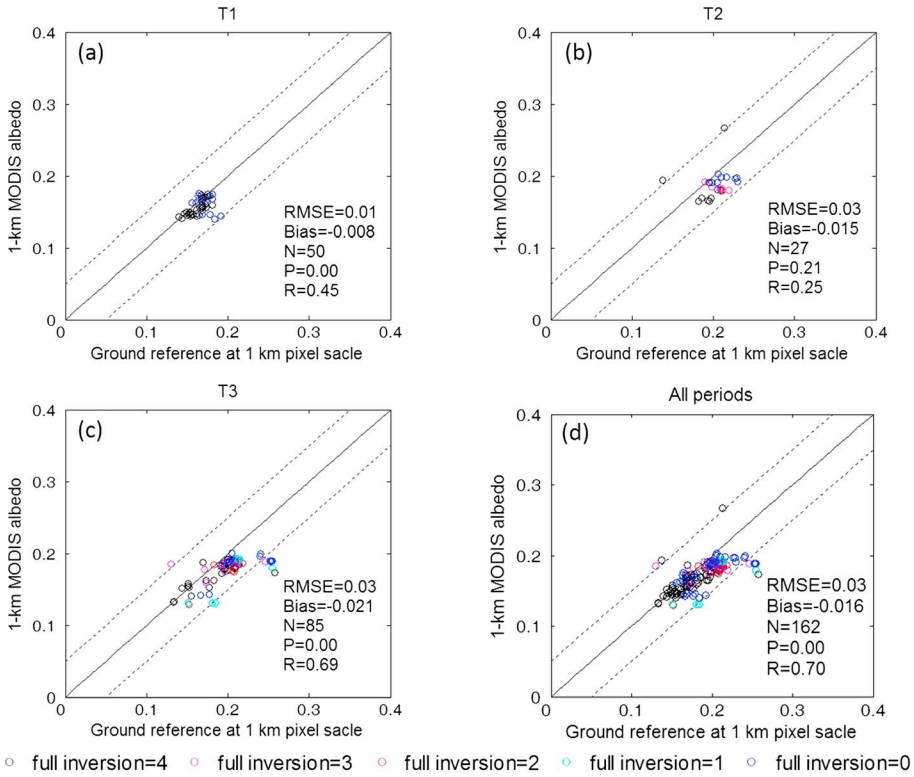

Figure 15. Scatterplot of the local noon ground reference at a 1 km pixel scale and the 1 km MODIS local noon albedos (V006) during the different periods. The different colors of circles indicate the different numbers of MCD43A3 (V006) pixels used in full inversion within the 1 km scale. The dotted lines show the bias on the interval [−0.05, 0.05].

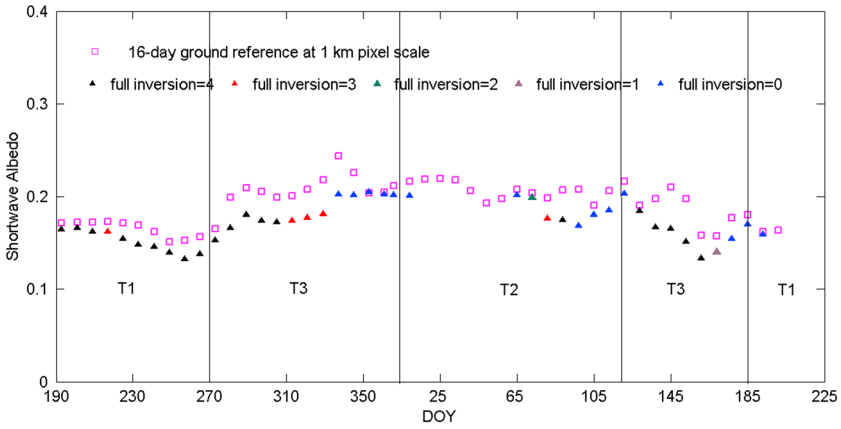

Figure 16. Comparisons between the 16 day 1 km ground reference and 1 km MODIS albedo (V005). Full inversion from 0 to 4 indicates the number of pixels from BRDF full inversions among the four MCD43A3 pixels within the 1 km scale.

albedo was not and affected by cloud detection and atmospheric effect. Second, the temporal variations in the surface albedo are better captured by VIIRS albedo, especially when abrupt change occurs. It shows that the STF method for GLASS albedo smoothens the albedo variations due to abrupt changes of land surfaces. Lastly, the VIIRS albedo temporal curve does not fluctuate sharply and is more temporally continuous than that of GLASS albedo.

Because of the difference in time and spatial resolutions of VIIRS and GLASS albedo, the comparison is just focused on their closeness with the ground reference at the corresponding pixel scale (Figure 13), but their absolute values are ignored. Their errors are both small during the vegetation-covered period (T1). However, it is apparent that the GLASS albedo shows larger errors than VIIRS albedo during the mixed cover (T3) and bare soil periods (T2), indicating that the VIIRS albedo outperforms GLASS albedo in depicting the surface albedo during these two periods, despite the dispersion of VIIRS albedo.

The different performance of VIIRS and GLASS albedos can be attributed to various factors. First, VIIRS and GLASS albedo were derived from different remote sensing data, and different instruments have different configurations with respect to spectral response functions and angular sampling domains. Second, the VIIRS albedo algorithm used TOA reflectances as input, whereas the GLASS albedo used here was derived from land surface reflectances. Lastly, although both albedos were generated using the direct-estimation algorithm, there were some procedural differences, such as the sizes of the bins in the regression procedure, as well as the applied aerosol models, surface BRDF databases, and band conversions used in the procedure to build the training data set.

As an inheritor of MODIS, it is imperative to carry out a comparison of the performance between VIIRS and MODIS albedo (V006) on a daily basis. The best agreement between MODIS albedo (V006) and ground reference is observed during T1 period (Figure 15a), with the smallest RMSE of 0.01. All of the errors are within ±0.05 with an average value of −0.008. Despite the relatively low R (0.45), a significant relationship exists between 1 km MODIS albedo (V006) and 1 km local noon ground references. The agreement is still good during the T3 period (Figure 15c), with a high R of 0.69 and most errors within ±0.05. However, the result of the comparison worsens during T2 (Figure 15b), and only a small number ($N = 27$) of MODIS albedos are available due to quality check processes. There is no significant correlation between MODIS albedo and ground reference with a small R of 0.25 and a large P of 0.21. When combining all periods, the overall RMSE and R are 0.03 and 0.70, respectively, and most data points are with errors less than 0.05 (Figure 15d). Nevertheless, as shown in Figure 14, the 1 km MODIS albedo (V006) almost systematically underestimates relative to the 1 km ground reference with an average bias of −0.016.

Table 3
Comparison of the Evaluation Results for the 16 day VIIRS Albedo and MCD43A3 (V005)

	16 day mean VIIRS albedo	MCD43A3 (V005)
RMSE	0.01	0.02
Bias	0.002	−0.02
R	0.87	0.85
P	0.00	0.00
N	48	41

Compared with Figures 4 and 6, it is apparent that VIIRS daily instantaneous albedo is inferior to the MODIS daily local noon albedo (V006) during the vegetation-covered period with respect to their agreements

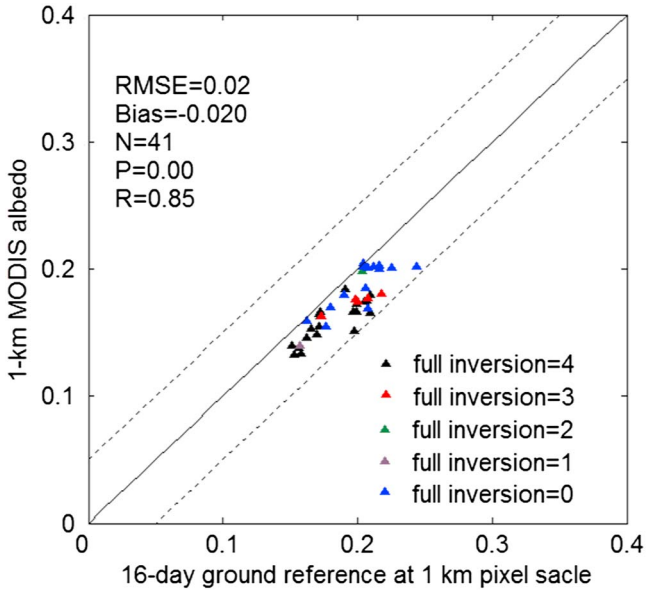

Figure 17. Scatterplot of the 16 day ground reference at a 1 km pixel scale and the 1 km MODIS albedos (V005) for the entire year. The different colors of triangles denote the different numbers of MCD43A3 (V005) pixels used in full inversion within the 1 km scale. The dotted lines show the bias on the interval [−0.05, 0.05].

with ground reference at corresponding pixel scale. VIIRS albedo shows a larger RMSE of 0.02 and lower R of 0.35 relative to ground reference than those of MODIS albedo (RMSE = 0.01, R = 0.45). Nevertheless, VIIRS albedo has distinct advantage over the 1 km MODIS albedo during bare-soil covered period by visually checking Figure 6b and Figure 15b. There are more albedo data available for VIIRS albedo (N = 54) than that of MODIS albedo (V006) (N = 27). Furthermore, the data points between VIIRS albedo and ground reference are on the line 1:1 with a very small average bias of −0.002, while that of MODIS albedo (V006) deviates from this line with a relatively large average bias of −0.015. And VIIRS albedo presents a smaller RMSE of 0.02 and a larger R of 0.41 than that of MODIS albedo (RMSE = 0.03, R = 0.25). The advantage of VIIRS albedo is still hold during the mixed-cover period, with a smaller RMSE of 0.02 and a comparable R of 0.62 than those of MODIS albedo (RMSE = 0.03, R = 0.69). In terms of the overall performance, VIIRS albedo also shows a higher accuracy, with a smaller RMSE of 0.02 and a slightly larger R of 0.73 than those of MODIS albedo (V006) (RMSE = 0.03, R = 0.70).

By comparing Figures 4 and 14, several differences between the performances of VIIRS albedo and MODIS albedo can be found. First, data missing occur in the MODIS daily local noon albedo, but not in the VIIRS daily instantaneous albedo. This may be associated with the less rigid quality control process of VIIRS albedo. Second, temporal sequence of the 1 km MODIS albedo is smoother than that of ground reference (1 km pixel scale), while the VIIRS albedo is more dispersed than that of ground reference (VIIRS pixel scale). Despite the smoothness of the MODIS albedo, it is inferior to VIIRS albedo in depicting the rapidly changing surface albedo. It is reasonable since the MODIS albedo (V006) was still using the 16 day retrieval algorithm despite the daily generation, thus losing detailed change in surface albedo. In contrast, the VIIRS albedo was based on daily instantaneous observations and therefore is more sensitive to the changes of the land surface. The comparison of their errors with respect to the ground reference shows their comparable performance since the differences between their errors are small (Figure 13).

4.2.2. Comparison With MODIS 16-Day Mean Albedo (V005)

The MCD43A3 (V006) is the latest version of MODIS albedo with the same temporal resolution as that of VIIRS albedo. However, the MCD43A3 (V005), with a temporal resolution of 8 days, is still the most extensively used and widely evaluated product now (Gascoin et al., 2017). In this paper, the V005 product was also used at a spatial resolution of 1 km for comparison with VIIRS 16 day mean albedo to demonstrate their characteristics.

The 1 km MODIS albedo (V005) is systematically lower than the ground reference (Figure 16), while their respective seasonal patterns are consistent, except for DOY 81 to 97 and DOY 129 to 145. These outliers are primarily caused by the serious surface albedo heterogeneity, which resulted from the frequent field

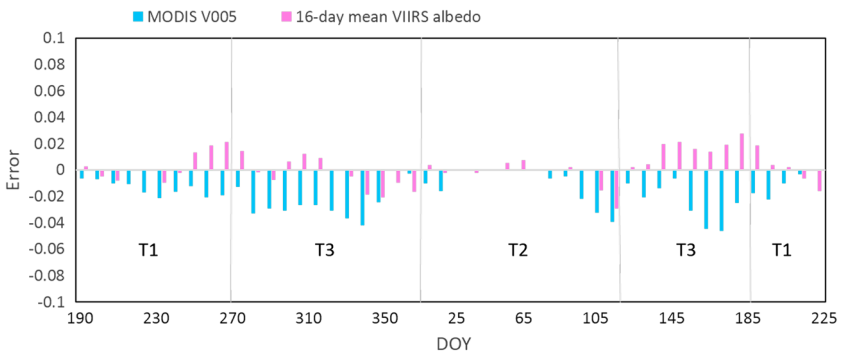

Figure 18. The comparison of the errors of MODIS local noon albedo (V005) and the 16 day mean VIIRS albedo with respect to the ground reference at corresponding pixel scales.

Table 4
Summary of Evaluation Results for VIIRS, GLASS, and MODIS Albedo During Different Periods

	T1 (vegetation period)			T2 (bare soil period)			T3 (mixed cover period)		
	VIIRS	GLASS	MCD43A3	VIIRS	GLASS	MCD43A3	VIIRS	GLASS	MCD43A3
RMSE	0.02	0.01	0.01	0.02	0.03	0.03	0.02	0.03	0.03
Bias	0.003	−0.007	−0.008	−0.002	−0.015	−0.015	0.005	−0.018	−0.021
N	42	50	50	54	43	27	73	94	85
P	0.02	0.00	0.00	0.00	0.81	0.21	0.00	0.00	0.00
R	0.35	0.71	0.45	0.41	0.04	0.25	0.62	0.60	0.69

managements (e.g., irrigation and fertilization). Additionally, the rapid change in surface albedo during the 16 day period corresponding to the 16 day MODIS product is also a contributor to their discrepancy.

The RMSE of the MODIS albedo (V005) is larger than that of 16 day mean VIIRS albedo (Table 3). However, its correlation with ground reference is similar to the 16 day mean VIIRS albedo. The magnitudes of the systematical underestimation of MODIS albedo (V005) relative to the 1 km ground reference are all less than 0.05 (Figure 17), with an average biases of −0.02, which is much larger than that of 16 day mean VIIRS albedo.

The lower RMSE of 16 day mean VIIRS albedo indicates that it is closer to the ground reference than that of 1 km MODIS albedo (V005). It is because both the 16 day ground reference and the 16 day VIIRS albedo are based on daily instantaneous observations, which may be more sensitive to rapid changes in surface conditions. By contrast, the MODIS albedo (V005) is based on 16 day accumulated observations, and its algorithm screened out obvious changes in the surface albedo. Therefore, the MODIS albedo (V005) will be biased when drastic changes of the land surfaces occur.

Comparison of the performance of 16 day mean albedo VIIRS albedo and MODIS albedo (V005) is shown in Figure 18. When the temporal resolution decreased from daily to 8 days, the magnitude of their errors reduced a lot (compared with Figure 13), showing that better closeness between albedo products and ground reference is attainable provided that the temporal resolution is sacrificed. Nevertheless, differences between the performances of VIIRS albedo and MODIS albedo (V005) grew. There is a clear distinction between the 16 day mean VIIRS albedo and 1 km MODIS albedo (V005) in terms of their closeness with the ground reference, especially during the mixed cover (T3) and bare soil periods (T2). The magnitude of MODIS albedo (V005) errors is mostly larger than that of the 16 day mean VIIRS albedo.

5. Conclusions

Preliminary assessments (Wang et al., 2013; Zhou et al., 2016) of VIIRS albedo have proved its acceptable accuracy. However, this kind of assessment suffers from uncertainties due to either the limited spatial representativeness of single site measurement or the complicated error sources when introducing intermediate spatial resolution imagery. This paper evaluated the accuracy of VIIRS granular-based albedo against ground reference at the VIIRS pixel scale over vegetation, bare soil, and mixed cover surfaces.

The ground reference at the VIIRS pixel was obtained by weighting the optimal multinode WSN-based measurements at the overpass time with the upscaling LUTs specified for the granule-based VIIRS albedo. It was qualified to represent the mean albedo within the VIIRS pixel throughout the year and thus was used as the most valid (unbiased) reference to directly evaluate the VIIRS albedo in long time series. The current granular VIIRS albedo has a high overall accuracy with a RMSE of 0.02 under the clear-sky condition, which is higher than that of MCD43A3 (V006) and GLASS albedo (Table 4). Further, it is generally significantly correlated with instantaneous ground references with a high R of 0.73.

During the vegetation-covered period, the VIIRS instantaneous albedo is inferior to MCD43A3 (V006) and GLASS local noon albedos, with a higher RMSE and a lower R. However, during the bare soil period, the VIIRS albedo shows distinct advantages over MODIS and GLASS albedos, as the correlation of VIIRS albedo with ground reference is much better than that of MODIS and GLASS albedos. During the mixed cover period, VIIRS albedo still retains its advantage over MODIS and GLASS albedos, with a smaller RMSE and a comparable R.

Although the VIIRS albedo is slightly dispersed in temporal sequence, which may be the result of the less rigid quality control process, it evidently outperforms GLASS and MODIS albedo in capturing the albedo temporal

variations, especially when land surface albedo reveals obvious day-to-day fluctuations. The VIIRS albedo also displays a better temporal continuity and shows no systematic error on the annual basis with an average bias of −0.002.

When resampling the VIIRS albedo into 16 day bins, the 16 day mean VIIRS albedo time series is smoother and more stable than that of VIIRS daily instantaneous albedo. The temporal trends of the 16 day mean VIIRS albedo and 16 day mean ground reference are more consistent with each other than the daily instantaneous product, and the RMSE is reduced when reducing the temporal resolution from daily to 8 days. These results indicate that the closeness between VIIRS albedo and ground reference can be improved when temporal resolution is sacrificed.

The highlights in this study should be acknowledged. First, not only relatively homogeneous land surfaces during vegetation and bare-soil periods but also heterogeneous land surfaces during a mixed-cover period were used to evaluate the VIIRS albedo. Therefore, the validation results are more comprehensive than that of only selecting representative sites for the evaluation. Second, a single point ground-observed albedo was not used since it would be insufficient to validate the albedo at spatial resolutions of approximately 1 km in the event of land surface heterogeneity. Instead, multipoint measurements were taken with high accuracy radiometers to capture the spatial-temporal variations of surface albedo in our experimental area. Thus, the validation results shown in this paper are more rigorous and reliable. Third, this paper provides an upscaling method specified for validation of VIIRS swath-based albedo, which also enhances the reliability of the validation results. Nevertheless, an accurate estimation of ground reference requires the inclusion of geometric errors of VIIRS images and the consideration of possible change in spatial resolution of VIIRS data for being targeted off-nadir, which are beyond the scope of this paper. Lastly, both the absolute accuracies relative to the pixel scale ground reference and the performance relative to the GLASS and MODIS were also given in this study.

Due to the limitations in the length of the ground measurement time series and the range of the experimental area, the validation was only conducted for a single year and in one area in this study. Thus, it just provides a preliminary assessment for VIIRS albedo product. It should also be noted that the upscaling method was based on the historical HJ albedo from 2010 and 2012. However, the surface coverage may change over a period of 3 years, which may introduce certain errors in the ground reference. Thus, the comparison results between VIIRS, GLASS, and MODIS albedo were associated not only with the different accuracies of themselves but also with the different accuracies of the ground reference at corresponding pixel scales. China is still working on the national validation network for remote sensing products, which will provide longer term ground measurements over more kinds of land cover in the future (Ma et al., 2015). We intend to continue the validation as more ground measurements become available.

Acknowledgments
This work was supported by Chinese Natural Science Foundation Project (41671363), the National Basic Research Program of China (2013CB733401), and the National High Technology Research and Development Program of China (2013AA12A301). We thank Dongdong Wang (Department of Geographical Sciences, University of Maryland, USA) for providing NPP VIIRS albedo over the experiment site and all the others who provide the validation data used in this study. They are the WSN's data provided by State Key Laboratory of Remote Sensing (available online at http://rsesdp.slrss.cn:9090/), the Huan Jing images provided by the China Center For Resources Satellite Data and Application (http://218.247.138.119:7777/DSSPlatform/index.html), the MODIS albedo products provided by NASA's Land Processes Distributed Active Archive Center (LP DAAC; https://e4ftl01.cr.usgs.gov/MOTA/), and the GLASS albedo provided by Beijing Normal University (http://glass-product.bnu.edu.cn/). Data analysis was conducted using the MATLAB programming languages. All the data presented in this manuscript will be made available through Coalition on Publishing Data in the Earth and Space Sciences (https://copdessdirectory.osf.io) and please e-mail J. Wen (wenjg@radi.ac.cn) for details.

References

Bicheron, P., & Leroy, M. (2000). Bidirectional reflectance distribution function signatures of major biomes observed from space. *Journal of Geophysical Reaearch*, *105*(D21), 26,669–26,681. https://doi.org/10.1029/2000JD900380

Cao, C., Luccia, F. J. D., Xiong, X., Wolfe, R., & Weng, F. (2013). Early on-orbit performance of the Visible Infrared Imaging Radiometer Suite onboard the Suomi National Polar-Orbiting Partnership (s-npp) satellite. *IEEE Transactions on Geoscience and Remote Sensing*, *52*(2), 1142–1156.

Cayula, J. F. P., Arnone, R. A., & Vandermeulen, R. A. (2015). Evaluation of VIIRS SST fields through the analysis of overlap regions between consecutive orbits. SPIE (Vol. 9459).

Cescatti, A., Marcolla, B., Santhana Vannan, S. K., Pan, J. Y., Román, M. O., Yang, X., & Schaaf, C. B. (2012). Intercomparison of MODIS albedo retrievals and in situ measurements across the global FLUXNET network. *Remote Sensing of Environment*, *121*, 323–334. https://doi.org/10.1016/j.rse.2012.02.019

Chen, Y. M., Liang, S., Wang, J., Kim, H. Y., & Martonchik, J. V. (2008). Validation of MISR land surface broadband albedo. *International Journal of Remote Sensing*, *29*(23), 6971–6983. https://doi.org/10.1080/01431160802199876

Cui, Y., Mitomi, Y., & Takamura, T. (2009). An empirical anisotropy correction model for estimating land surface albedo for radiation budget studies. *Remote Sensing of Environment*, *113*(1), 24–39. https://doi.org/10.1016/j.rse.2008.08.007

Dou, B., Wen, J., Li, X., Liu, Q., Peng, J., & Xiao, Q. (2016). Wireless sensor network of typical land surface parameters and its preliminary applications for coarse-resolution remote sensing pixel. *International Journal of Distributed Sensor Networks*, *12*(3), 1–11.

Gao, F., Schaaf, C. B., Strahler, A. H., Roesch, A., Lucht, W., & Dickinson, R. (2005). MODIS bidirectional reflectance distribution function and albedo climate modeling grid products and the variability of albedo for major global vegetation types. *Journal of Geophysical Research*, *110*, D01104. https://doi.org/10.1029/2004JD005190

Gascoin, S., Guðmundsson, S., Aðalgeirsdóttir, G., Pálsson, F., Schmidt, L., Berthier, E., & Björnsson, H. (2017). Evaluation of MODIS albedo product over ice caps in Iceland and impact of volcanic eruptions on their albedo. *Remote Sensing*, *9*(5), 399. https://doi.org/10.3390/rs9050399

Govaerts, Y., Lattanzio, A., Taberner, M., & Pinty, B. (2008). Generating global surface albedo products from multiple geostationary satellites. *Remote Sensing of Environment*, *112*(6), 2804–2816. https://doi.org/10.1016/j.rse.2008.01.012

Govaerts, Y. M., Wagner, S., Lattanzio, A., & Watts, P. (2010). Joint retrieval of surface reflectance and aerosol optical depth from MSG/SEVIRI observations with an optimal estimation approach: 1. Theory. *Journal of Geophysical Research*, *115*, D02203. https://doi.org/10.1029/2009JD011779

He, T., Liang, S. L., Wang, D. D., Wu, H. Y., Yu, Y., & Wang, J. D. (2012). Estimation of surface albedo and directional reflectance from Moderate Resolution Imaging Spectroradiometer (MODIS) observations. *Remote Sensing of Environment*, *119*, 286–300. https://doi.org/10.1016/j.rse.2012.01.004

He, T., Liang, S., & Song, D. (2014). Analysis of global land surface albedo climatology and spatial-temporal variation during 1981–2010 from multiple satellite products. *Journal of Geophysical Research: Atmospheress*, *119*, 10,281–10,298. https://doi.org/10.1002/2014JD021667

Kotchenova, S. Y., Vermote, E. F., Matarrese, R., & Jr, K. F. (2006). Validation of a vector version of the 6s radiative transfer code for atmospheric correction of satellite data, part I: Path radiance. *Applied Optics*, *45*(26), 6762–6774. https://doi.org/10.1364/AO.45.006762

Leeuwen, W. J. D. V., & Roujean, J. L. (2002). Land surface albedo from the synergistic use of polar (eps) and geo-stationary (msg) observing systems: An assessment of physical uncertainties. *Remote Sensing of Environment*, *81*(2-3), 273–289. https://doi.org/10.1016/S0034-4257(02)00005-6

Li, X. W., & Strahler, A. H. (1992). Geometric-optical bidirectional reflectance modeling of the discrete crown vegetation canopy: Effect of crown shape and mutual shadowing. *IEEE Transactions on Geoscience and Remote Sensing*, *30*(2), 276–292. https://doi.org/10.1109/36.134078

Li, Y., Sheng, S., & Zhao, X. (2012). Application of MODIS albedo data in the simulation of air temperature over Beijing. *Journal of the Meteorological Sciences*, *32*(6), 622–628.

Liang, S. (2003). A direct algorithm for estimating land surface broadband albedos from MODIS imagery. *IEEE Transactions on Geoscience and Remote Sensing*, *41*(1), 136–145. https://doi.org/10.1109/TGRS.2002.807751

Liang, S. (2004). *Quantitative remote sensing of land surfaces*. Hoboken: John Wiley.

Liang, S., Strahler, A. H., & Walthall, C. (1999). Retrieval of land surface albedo from satellite observations: A simulation study. *Journal of Applied Meteorology*, *38*(6), 712–725. https://doi.org/10.1175/1520-0450(1999)038%3C0712:ROLSAF%3E2.0.CO;2

Liang, S., Stroeve, J., & Box, J. E. (2005). Mapping daily snow/ice shortwave broadband albedo from Moderate Resolution Imaging Spectroradiometer (MODIS): The improved direct retrieval algorithm and validation with Greenland in situ measurement. *Journal of Geophysical Research*, *110*, D10109. https://doi.org/10.1029/2004JD005493

Liang, S., Yu, Y., & Defelice, T. P. (2005). VIIRS narrowband to broadband land surface albedo conversion: Formula and validation[J]. *International Journal of Remote Sensing*, *26*(5), 1019–1025. https://doi.org/10.1080/01431160512331340156

Liu, J., Schaaf, C., Strahler, A., Jiao, Z., Shuai, Y., Zhang, Q., & Dutton, E. G. (2009). Validation of Moderate Resolution Imaging Spectroradiometer (MODIS) albedo retrieval algorithm: Dependence of albedo on solar zenith angle. *Journal of Geophysical Research*, *114*, D01106. https://doi.org/10.1029/2008JD009969

Liu, Q., Wang, L., Qu, Y., Liu, N. F., Liu, S., Tang, H., & Liang, S. (2013). Preliminary evaluation of the long-term GLASS albedo product[J]. *International Journal of Digital Earth*, *6*(sup1), 69–95. https://doi.org/10.1080/17538947.2013.804601

Liu, N. F., Liu, Q., Wang, L. Z., Liang, S. L., Wen, J. G., Qu, Y., & Liu, S. H. (2013). A statistics-based temporal filter algorithm to map spatio-temporally continuous shortwave albedo from MODIS data. *Hydrology and Earth System Sciences*, *17*(6), 2121–2129. https://doi.org/10.5194/hess-17-2121-2013

Lucht, W., Hyman, A. H., Strahler, A. H., Barnsley, M. J., Hobson, P., & Muller, J. P. (2000). A comparison of satellite-derived spectral albedos to ground-based broadband albedo measurements modeled to satellite spatial scale for a semidesert landscape. *Remote Sensing of Environment*, *74*(1), 85–98. https://doi.org/10.1016/S0034-4257(00)00125-5

Lucht, W., Schaaf, C. B., & Strahler, A. H. (2002). An algorithm for the retrieval of albedo from space using semiempirical BRDF models. *IEEE Transactions on Geoscience and Remote Sensing*, *38*(2), 977–998. https://doi.org/10.1109/36.841980

Ma, M., Che, T., Li, X., Xiao, Q., Zhao, K., & Xin, X. (2015). A prototype network for remote sensing validation in china. *Remote Sensing*, *7*(5), 5187–5202. https://doi.org/10.3390/rs70505187

Mira, M., Weiss, M., Baret, F., Courault, D., Hagolle, O., Gallego-Elvira, B., & Olioso, A. (2015). The MODIS (collection v006) BRDF/albedo product MCD43D: Temporal course evaluated over agricultural landscape. *Remote Sensing of Environment*, *170*, 216–228. https://doi.org/10.1016/j.rse.2015.09.021

Muller, J. (2008, Dec. 1). BRDF/albedo retrieval CA [online]. Retrieved from http://www.brockmann-consult.de/albedomap/documentation.html

Muller, J. P., Zuhlke, M., Brockmann, C., Preusker, R., Fischer, J., & Regner, P. (2007). ALBEDOMAP: MERIS land surface albedo retrieval using data fusion with MODIS BRDF and its validation using contemporaneous EO and in situ data products. Geoscience and Remote Sensing Symposium (IGARSS), 2007 IEEE International, 2404–2407.

Peng, J. J., Liu, Q., Wen, J. G., Liu, Q. H., Tang, Y., Wang, L. Z., … Shi, J. (2014). Multi-scale validation strategy for satellite albedo products and its uncertainty analysis. *Science China: Earth Sciences*, *58*, 573–588. https://doi.org/10.1007/s11430-014-4997-y

Privette, J. L., Schaaf, C. B., Saleous, N., & Liang, S. (2004). Evaluation of operational albedo algorithms for AVHRR, MODIS and VIIRS: Case studies in Southern Africa. American Geophysical Union, Fall Meeting, Abstract B33D-03.

Qu, Y., Liu, Q., Liang, S. L., Wang, L. Z., Liu, N. F., & Liu, S. H. (2014). Direct-estimation algorithm for mapping daily land-surface broadband albedo from MODIS data. *IEEE Transactions on Geoscience and Remote Sensing*, *52*(2), 907–919. https://doi.org/10.1109/TGRS.2013.2245670

Román, M. O., Schaaf, C. B., Woodcock, C. E., Strahler, A. H., Yang, X., Braswell, R. H., & Wofsy, S. C. (2009). The MODIS (Collection V005) BRDF/albedo product: Assessment of spatial representativeness over forested landscapes. *Remote Sensing of Environment*, *113*(11), 2476–2498. https://doi.org/10.1016/j.rse.2009.07.009

Roman, M. O., Gatebe, C. K., Shuai, Y., Wang, Z., Gao, F., Masek, J. G., … Schaaf, C. B. (2013). Use of in situ and airborne multiangle data to assess MODIS- and Landsat-based estimates of directional reflectance and albedo. *IEEE Transactions on Geoscience and Remote Sensing*, *51*(3), 1393–1404. https://doi.org/10.1109/TGRS.2013.2243457

Ross, J. (1981). *The radiation regime and architecture of plant stands*. The Hague, Netherlands: Junk Publishers. https://doi.org/10.1007/978-94-009-8647-3

Sailor, D. J., Resh, K., & Segura, D. (2006). Field measurement of albedo for limited extent test surfaces. *Solar Energy*, *80*(5), 589–599. https://doi.org/10.1016/j.solener.2005.03.012

Saunders, R. W. (1990). The determination of broad band surface albedo from AVHRR visible and near-infrared radiances. *International Journal of Remote Sensing*, *11*(1), 49–67. https://doi.org/10.1080/01431169008955000

Schaaf, C. B., Gao, F., Strahler, A. H., Lucht, W., Li, X., Tsang, T., … Roy, D. (2002). First operational BRDF, albedo nadir reflectance products from MODIS. *Remote Sensing of Environment*, *83*(1-2), 135–148. https://doi.org/10.1016/S0034-4257(02)00091-3

Schaaf, C. B., Wang, Z., & Strahler, A. H. (2011). Commentary on Wang and Zender-MODIS snow albedo bias at high solar zenith angles relative to theory and to in situ observations in Greenland. *Remote Sensing of Environment*, *115*(5), 1296–1300. https://doi.org/10.1016/j.rse.2011.01.002

Shi, X., Wen, J., Tian, H., Wang, L., Zhang, T., Liu, R., … Zhang, J. (2009). Application of MODIS albedo data in the simulation of land surface and rainfall processes over the Yellow River water source region. *Chinese Journal of Atmospheric Sciences (in Chinese)*, *33*(6), 1187–1200.

Strugnell, N. C., Lucht, W., & Schaaf, C. (2001). A global albedo data set derived from AVHRR data for use in climate simulations. *Geography Research Letters*, *28*(1), 191–194. https://doi.org/10.1029/2000GL011580

Wang, X. W., & Zender, C. S. (2010). MODIS snow albedo bias at high solar zenith angles relative to theory and to in situ observation in Greenland. *Remote Sensing of Environment*, *114*(3), 563–575. https://doi.org/10.1016/j.rse.2009.10.014

Wang, Z., Schaaf, C. B., Chopping, M. J., Strahler, A. H., Wang, J., Román, M. O., … Shuai, Y. M. (2012). Evaluation of Moderate-Resolution Imaging Spectroradiometer (MODIS) snow albedo product (MCD43A) over tundra. *Remote Sensing of Environment*, *117*, 264–280. https://doi.org/10.1016/j.rse.2011.10.002

Wang, D. D., Liang, S. L., He, T., & Yu, Y. (2013). Direct estimation of land surface albedo from VIIRS data: Algorithm improvement and preliminary validation. *Journal of Geophysical Research*, *118*, 577–12,586.

Wang, Z., Schaaf, C. B., Strahler, A. H., Chopping, M. J., Román, M. O., Shuai, Y., … Fitzjarrald, D. R. (2014). Evaluation of MODIS albedo product (MCD43A) over grassland, agriculture and forest surface types during dormant and snow-covered periods. *Remote Sensing of Environment*, *140*, 60–77. https://doi.org/10.1016/j.rse.2013.08.025

Wanner, W., Strahler, A. H., Hu, B., Lewis, P., Muller, J. P., Li, X., … Barnsley, M. J. (1997). Global retrieval of bidirectional reflectance and albedo over land from EOS MODIS and MISR data: Theory and algorithm. *Journal of Geophysical Research*, *102*(D14), 17,143–17,161. https://doi.org/10.1029/96JD03295

Wu, X., Wen, J., Xiao, Q., Liu, Q., Peng, J., Dou, B. C., … Liu, Q. H. (2016). Coarse scale in situ albedo observations over heterogeneous snow-free land surfaces and validation strategy: A case of MODIS albedo products preliminary validation over northern China. *Remote Sensing of Environment*, *184*, 25–39. https://doi.org/10.1016/j.rse.2016.06.013

You, D., Wen, J. G., Xiao, Q., Liu, Q., Peng, J. J., Liu, Q. H., … Dou, B. C. (2015). Development of a high resolution BRDF/albedo product in the oasis area of the Heihe River Basin by fusing if airborne CASI reflectance with MODIS daily reflectance. *Remote Sensing*, *7*(6), 6784–6807. https://doi.org/10.3390/rs70606784

Yu, Y., Privette, J. L., & Pinheiro, A. C. (2008). Evaluation of split-window land surface temperature algorithms for generating climate data records. *IEEE Transactions on Geoscience and Remote Sensing*, *46*(1), 179–192. https://doi.org/10.1109/TGRS.2007.909097

Zhou, Y., Wang, D., Liang, S., Yu, Y., & He, T. (2016). Assessment of the Suomi NPP VIIRS land surface albedo data using station measurements and high-resolution albedo maps. *Remote Sensing*, *8*(2), 137. https://doi.org/10.3390/rs8020137